Mechanics of Materials 153 (2021) 103673

Contents lists available at ScienceDirect

Mechanics of Materials

journal homepage: www.elsevier.com/locate/mechmat

Mechanical design of ring tensile specimen via surrogate modelling for inverse material parameter identification

Zied Ktari [a], Carlos Leitão [b], Pedro A. Prates [b], Ali Khalfallah [a,b,c,*]

[a] Laboratoire de Génie Mécanique, Ecole Nationale d'Ingénieurs de Monastir, Av. Ibn Eljazzar Monastir, 5019, Université de Monastir, Tunisia
[b] CEMMPRE, Department of Mechanical Engineering, University of Coimbra, Rua Luis Reis Santos, Pinhal de Marrocos, 3030-788, Coimbra, Portugal
[c] Institut Supérieur des Sciences Appliquées et de Technologie de Sousse, Cité Ibn Khaldoun, 4003, Sousse, Université de Sousse, Tunisia

ARTICLE INFO

Keywords:
Ring tensile test
Mechanical design
Surrogate modelling
Finite element analysis
Parameter identification
Anisotropy

ABSTRACT

The mechanical characterization of anisotropic thin walled-tubes along hoop direction is not a trivial task. It is necessary to develop experimental techniques, numerical methods and design test samples, which enable to determine the real tube properties along hoop direction without any external influences. In this study, first we propose a surrogate based-model for the mechanical design of the ring hoop tensile test (RHTT) specimen, in order to obtain the effective homogeneous stress and strain distribution of the uniaxial tensile test along hoop direction. Second, the optimized sample is used to carry out RHTT and to obtain the actual flow stress curve and the anisotropy coefficients of AA6063-O extruded tube. However, the experimental curve measured from RHTT (force –displacement) is a degenerate response, since it suffers from intermixture effects of the effective material behaviour with the friction between the sample and the sample-holding tool. Hence, we developed an inverse parameter identification method, which uses design of experiments, finite element analysis and artificial neural network to separate out the tubular material parameters from the friction coefficient. The assessment of the developed method is achieved by comparing the predicted material parameters and the identified flow stress curve obtained by artificial neural network algorithm. The finite element simulation results corroborate the obtained findings.

1. Introduction

In recent years, there have been several attempts to conduct shape optimization of test specimens to attain homogeneous distribution of stress-strain within these specimens, such as shear test, plane strain test and equi-biaxial test (Bouvier et al., 2006; Pereira et al., 2015). There is an alternative to homogeneous tests, where the shape optimization is needed to design some specific samples for heterogeneous tests (Prates et al., 2014; Souto et al., 2014). The chief aim of all these research activities is to acquire effective experimental results, which represent a known and defined strain and stress field distribution that can be used to identify the material parameters and anisotropy of metal sheets. In the same way, the mechanical characterization of thin-walled tubular materials is not a trivial task as sheet metals; obviously, since tubes are not flat shapes as sheets. However, simple methods are still practiced based on specimens cut off from flattened tubes and then tested in uniaxial tensile (Zribi et al., 2013; Pierron et al., 2003). Nevertheless, in turn, the flattening operation induces pre-strains, residual stresses within the material, which ultimately affects the material behaviour of tubes and then the material parameter identification accuracy (Saikaly et al., 1996; Dick and Korkolis, 2014). In order to overcome such drawbacks, meticulous researchers have proposed the so-called Ring Hoop Tensile Test (RHTT), which was originally dedicated for determining the hoop mechanical properties of thermoplastic tubular materials (ASTM D2290, 2003). The main advantage of the RHTT technique is the assessment of the tubular material properties along the hoop direction of as-received metallic tubes, thus avoiding unnecessary work hardening by flattening operation. In this context, Price (1972) is the first researcher who proposed in 1972 the RHTT technique to investigate the effect of the precipitation of hydrides in internally pressurized tubes made of Zircaloy on the resistance of fracture at high temperature. He employed a ring specimen with a single reduced section that has a gauge length $l = 25.4$ mm and a gauge width $w = 6.35$ mm. Mehan et al. (1987) employed the ring hoop test to evaluate the mechanical properties in the hoop

* Corresponding author: CEMMPRE, Department of Mechanical Engineering, University of Coimbra, Rua Luis Reis Santos, Pinhal de Marrocos, 3030-788, Coimbra, Portugal.
E-mail addresses: ali.khalfallah@dem.uc.pt, ali.khalfallah@dem.uc.pt (A. Khalfallah).

https://doi.org/10.1016/j.mechmat.2020.103673
Received 8 April 2020; Received in revised form 18 November 2020; Accepted 21 November 2020
Available online 29 November 2020

Table 1
Comparative overview of the RHTT specimen geometries available in the literature for characterizing tubular metallic materials.

Authors	Year	Length, l (mm)	Width, w (mm)	Fillet radius, r (mm)	Single/double gauge	Tube diameter/thickness (mm)	Material
Barsoum and Al Ali (2015)	2015	9.5	3	6	single	60/3	AA 6063-T5
Dick and Korkolis (2014)	2014	24	6.35	6.35	single	60/3	AA 6061-T4
Samal et al. (2013)	2013	20	6	3.25	Single	83/4.3	Zircaloy4
		25	6	3.25	Single	83/4.3	Zr-2.5Nb Alloy
Arzaghi et al. (2012)	2012	8	3	1.5	single	20/1	AA 1050
Martín-Rengel et al., 2012	2012	5	2	1.5	double	9.5/0.57	Zircaloy4
(Kim et al., 2012)	2012	4	2	1.5	double	9.68/0.62	Zircaloy4
Lin et al. (2011)	2011	25	5	7.5	single	44/1.8	AZ31B alloy
He et al. (2010)	2010	25	5	7.5	single	44/1.8	AZ31B alloy
Kim et al. (2009)	2009	4	2	1	double	9.5/0.57	Zircaloy4
Nagase et al. (2009)	2009	3	2	1	double	9.5/0.57	Zircaloy4
Lee et al. (2009)	2009	4	2	1	double	9.5/0.57	Zircaloy4
Jiang et al. (2008)	2008	33	6.4	1	single	70/4	AM30-AZ31
Seok et al. (2006)	2006	2	2	1.5	double	9.5/0.57	Zircaloy4
Yoshitake et al. (2004)	2004	2	1,5	1.5	double	9.3/0.6	Martensitic Steel
Daum et al. (2002)	2002	4.06	1.02	1.02	double	10.9/0.71	Zircaloy4
Grigoriev et al. (2002)	2002	2	2	3	double	9.5/0.57	Zircaloy2
		3	2	3	double	12.5/1	
Bates et al. (2000)	2000	5.28	2,13	1.57	double	9.52/0.57	Zircaloy4
Cohen et al. (1998)	1998	2.11	1.7	1.08	double	9.5/0.57	Zircaloy4
Link et al. (1998)	1998	6.35	1.01	1.01	double	9.52/0.57	Zircaloy4
(Arsène and Bai, 1996)	1996	2	2	1.5	double	9.62/0.36	Zircaloy2
Price (1972)	1972	25.4	6.35	6.35	single	105.15/4.19	Zircaloy2

direction of a low-pressure plasma-deposited nickel-base super-alloy, at temperature ranging between 25 °C and 1010 °C. The authors have utilized four ring geometries, where two of them have a reduced gauge section with the following sizes $w = 2.8$ mm and $l = 12.8$ mm. Arsène and Bai (1996) studied the effect of the friction between the ring and the D-shaped block, and proposed a new RHTT, which combines double-D mandrels and a dog-bone insert. They also examined the effect of the sample geometry on the uniformity of the stress distribution. Link et al. (1998) designed a large RHTT specimen configuration in which near plane-strain deformation is achieved to examine the ductility of Zircaloy-4 cladding tubes. Wang et al. (2002) developed a ring hoop tensile test to avoid the flattening of ring specimens and to determine the hoop stress-strain curve of thin-walled tubular materials. Jiang et al. (2008) performed at warm temperature the RHTT on ring samples taken from two magnesium-based alloy tubes. The authors chose a specimen with a single reduced section, and have a length-to-width ratio (l/w) equal to 5.15. He et al. (2010) and Lin et al. (2011) have carried out a ring hoop tensile test on specimens with $l/w = 5$ to evaluate the formability of AZ31B magnesium alloy tube at warm temperature. Later, Samal et al. (2013) used a ring specimen having a reduced cross section with l/w = 4.16. Dick and Korkolis (2014) performed the ring hoop tensile test on specimen having a dog bone-shaped section with $l/w =$ 3.78, stating that such ratio would be suitable for the RHTT specimens. Barsoum and Al Ali (2015) run numerical analyses in order to design RHTT samples with $l/w = 3.16$ and a fillet radius $r = 6$ mm. They obtained using trial-and-error method, the friction coefficient between the ring and the supporting D-shaped block. Nagase et al. (2009) performed analytical and experimental investigations for shape optimization of RHTT samples to measure the mechanical properties of the Zircaloy cladding in the hoop direction. They designed a ring specimen with a single gauge section, which is mounted on the D-shaped blocks to reduce the undesirable friction and bending effects. They chose a gauge length-to-width ratio between 1.5 and 2. Such length-to-width ratio (l/w) is about half of the value for which the uniaxial tensile stress state is reached. Pierron et al. (2003) examined the influence of tensile specimen geometries on the deformation behaviour of a flattened Zircaloy-4 tube for gauge length-to-width ratio (l/w) that ranges between 1 and 4. The authors state that the strain distribution at maximum load are uniform only in the specimen geometry with $l/w = 4$.

According to this literature review, it was noticed that several researchers have attempted to use different ring specimen geometries to investigate the material behaviour in the hoop direction of metallic tubes. Table 1 shows a comparative outline of these geometries. Since there is no standard or a single design of metallic RHTT specimen,

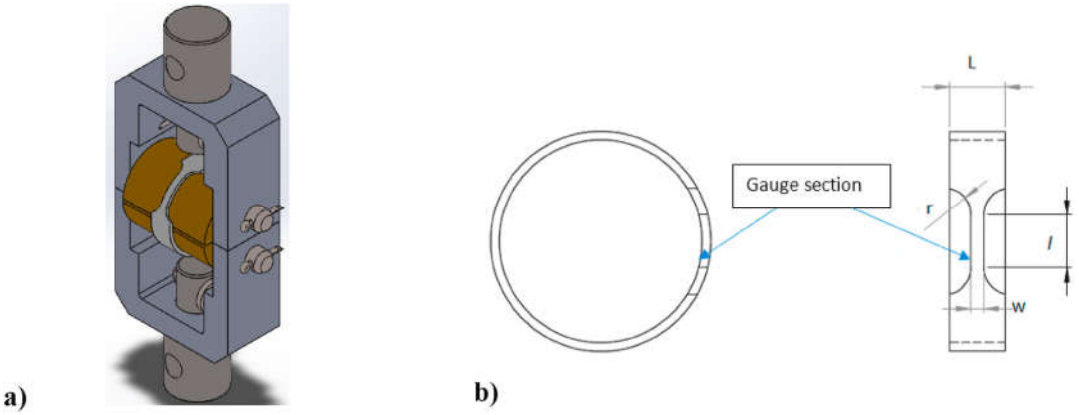

Fig. 1. a) 3D drawing design of the fixture tool for RHTT; b) Design variables which define the Geometry and dimensions of the gauge zone for the ring hoop tensile specimen.

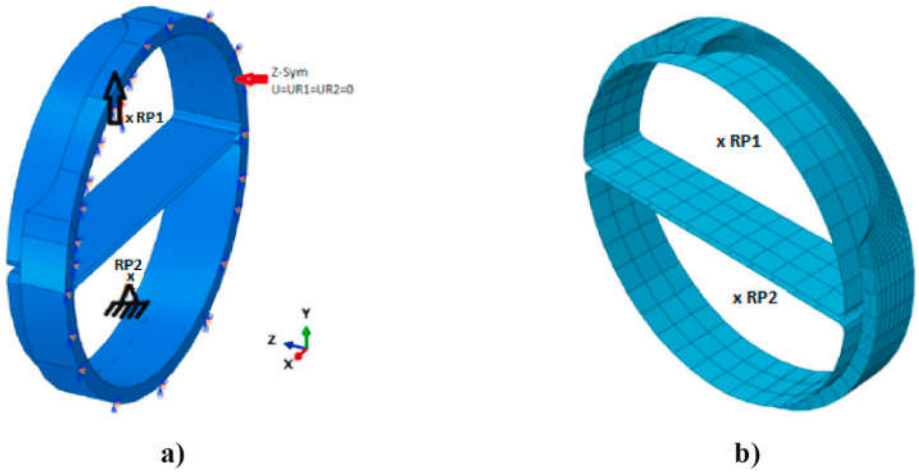

Fig. 2. Half of the RHTT finite element model: D-shaped blocks are modelled as analytic rigid shell for which reference points RP_1 and RP_2 are assigned to define the boundary conditions. The ring is modelled as a deformable 3D body: a) CAD model of RHTT along with the assignment of boundary conditions; b) mesh of the finite element model: the ring is meshed with a size of 1 mm and refinement in the gauge section with element size of 0.3 mm. Five elements are used across the ring thickness.

generally, the proposed dimensions in the literature are miscellaneous and authors didn't demonstrate, in general, whether the used ring specimens experience uniaxial tensile strain and stress states or not. In addition, the friction between the ring sample and the tooling tampers the resulting mechanical properties along the hoop direction. Some authors neglect the friction effect or assumed it very small (Jiang et al., 2008; Nagase et al., 2009), and solely rare works attempted to determine the friction coefficient using trivial trial and error method (Barsoum and Al Ali, 2015).

The aim of this work is to propose an effective surrogate based-model for the mechanical design of a sample geometry, which should experience an homogeneous uniaxial tensile stress state in the gauge section during RHTT. In addition, experimental tests are conducted on the optimized RHTT geometry to characterize the mechanical behaviour and anisotropy of AA6063-O aluminium alloy. Strain fields are measured during the RHTT using stereo Digital Image Correlation (DIC) system. Because of the occurrence of friction between the ring specimen and the tool (D-shaped blocks), the resulting RHTT response is prone to errors, so-called a degenerate response. In order to determine effective material properties from this degenerate response, an artificial neural network (ANN) is constructed to derive accurately the flow stress curve in the hoop direction. The advantage of the proposed method is that it separates out the flow stress parameters and the friction coefficient from the experimental RHTT force –displacement curve. The cause of this degeneracy is the intermixture effects of the actual material properties and friction. To assess the developed method ability to segregate the mechanical behaviour and the friction from the RHTT degenerate response, comparison between the predicted material behaviour using Hill48 yield criterion and the real flow stress curve was performed. A good agreement is attained and the finite element analysis results substantiated the obtained findings.

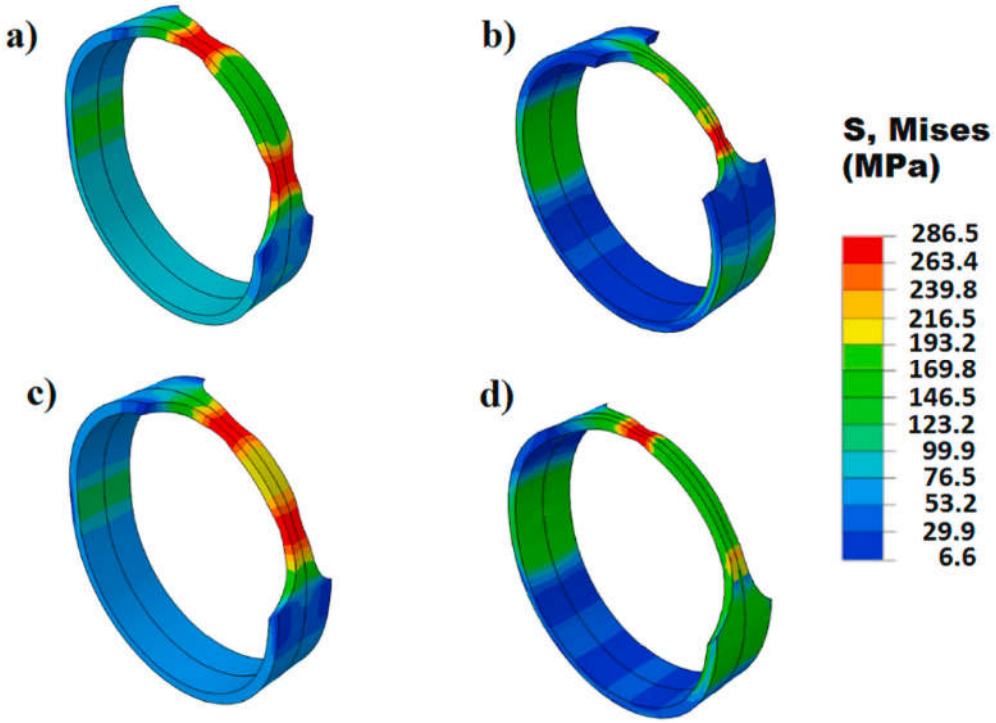

Fig. 3. Contours of von Mises equivalent stress obtained from ring hoop tensile test simulations using four given sets of the design variables (*l,w,r*) of the RHTT samples: a) ($l = 24$, $w = 6$, $r = 6$); b) ($l = 15$, $w = 3$, $r = 4$); c) ($l = 20$, $w = 4$, $r = 6$); d) ($l = 24$, $w = 3$, $r = 8$); (Units in mm).

2. Finite element simulation

Commercial finite element ABAQUS/Standard code is used to run numerical simulation of ring samples with one gauge section, which is inserted within two half-cylindrical blocks, commonly called as D-shaped blocks, as seen in Fig. 1a. An initial tiny gap between the two D-shaped block halves of about 1 mm was considered. Fig. 1b shows the drawing design of the ring hoop tensile specimen with the dimensions that define the sample geometry for RHTT. In this section, the finite element model is described in details and the design parameters that describe the ring sample geometry are given.

For the RHTT sample, the design variables (l), (w) and (r) denote the cord length, the width of the gauge section, and the fillet radius, respectively.

Taking account of the symmetry of geometry, material, and boundary conditions, a half of the whole FE model is considered. Fig. 2 shows the finite element (FE) model of the RHTT sample. A symmetric boundary condition (ZSYM) is assigned to the lateral surface of the ring as depicted in Fig. 2a. The upper and lower D-shaped blocks are modelled as analytic rigid shell and defined by the reference points RP1 and RP2, respectively. The ring is modelled as a deformable 3D body. The outer diameter and the initial thickness of the tube are 50 mm and 2 mm, respectively. Three dimensional 8-node hexahedral continuum elements (C3D8R) with reduced integration were used to mesh the ring with a size of 1 mm and refinement in the gauge section with elements size of 0.3 mm. Five elements have been used across the ring thickness to effectively capture the evolution of the radial stress and strain (Fig. 2b). Whereas, the D-shaped blocks were meshed with bilinear 4 node rigid quadrilateral elements (R3D4). The specimen gauge centre is oriented at about 45° from the vertical axe, so that the gauge section is completely in contact with the outer surface of the upper D-shaped block. This configuration also avoids the occurrence of bending moment in the ring section during the RHTT, and the plastic deformation accumulated during the RHTT is better localized within the sample's gauge.

A contact interaction of master-slave type is defined between the outer surface of the D-shaped block (Master) and the inner surface of the ring (Slave). This contact is characterized by normal behaviour "Hard Contact" and a Coulomb-type friction with a chosen coefficient of friction $\mu = 0.08$ (reasonable value), to generally mimic experimental conditions. The ring hoop tensile test is conducted in two steps. In the first step, the initial gap between each D-shaped block and the ring is enclosed by a slight displacement of the two rigid mandrels ensuring contact. In the second step, the lower D-shaped block is maintained immovable, while the upper D-shaped block moves upwards and tighten to its reference point. Consequently, the ring gauge section is stretched along the circumferential direction. For a first attempt, the material behaviour adopted in the numerical simulation used in the sample shape optimization is the rate-independent J_2 flow theory of plasticity with isotropic hardening and an associated flow rule.

In order to illuminate the necessity to carry out the shape optimization of the RHTT specimen to ensure that the strain and stress fields fulfilled the uniaxial tensile state, we have used four hazardous sets of the design variables (l,w,r) that define the geometry of the ring sample to run FE simulation of RHTT. Fig. 3a, b, 3c, and 3d show the contours of von Mises equivalent stress obtained from simulation results. It can be observed that the various design variables have serious implications on the stress distribution within the specimen's gauge section. Moreover, the necking could occur in one or in other extremity or/and in both locations of the ring specimen's gauge section.

Based on these finite element results, it is clearly demonstrated that design variables (l,w,r) of the RHTT specimen shape has serious effects on the location of necking and then on the stress and strain distribution. Thus, the optimal sample's shape of the RHTT should be determined by seeking the nominal design variables using simultaneous optimization of multiple responses. The optimization method used is a statistical technique based on the multiple regression equations that relate the input design variables to the target outputs.

Table 2
Target outputs for the design variables of RHTT shape optimization to obtain homogeneous stress and strain distribution in the uniaxial tensile test along hoop direction.

Response	Target output values
Strain path $\rho = \frac{\varepsilon_{zz}}{\varepsilon_{\theta\theta}}$	−0.5
Stress path x $= \frac{\sigma_{zz}}{\sigma_{\theta\theta}}$	0
Lode parameter L	−1
Stress Triaxiality Σ	1/3

3. RHTT shape optimization methodology

Since there is no standardization of RHTT specimen used for metallic tubes and pipes characterization, then we are focusing on the shape optimization of the ring specimen. The chief concerns is that the specimen gauge should undergoes uniaxial tensile stress state during RHTT. The shape optimization is based on the design of experiment method (DoE) and the FE simulation with multiple regression technique. A set of the FE simulation results is generated based on the DoE method. Then, a surrogate modelling method, such as the response surface method (RSM) is used to extract the optimal design variables. The RSM is a statistical and mathematical method, which is an operative method for design optimization for analysing empirical relationships. This method has been widely employed in the optimization of many manufacturing processes, such as bending, stamping and among others, (Hambli, 2002; Bahloul et al., 2006). In order to optimize the design variables defining the shape and dimensions of the RHTT sample, the RSM is used to express the relationship between the independent design variables (l,w,r) and target outputs (x, ρ, Σ, Lode parameter) using regression technique. These latter parameters, which define the strain path $\rho = (\varepsilon_{zz}/\varepsilon_{\theta\theta})$, the stress path$x = (\sigma_{zz}/\sigma_{\theta\theta})$, the stress triaxiality Σ and the Lode parameter L, are chosen as the criteria that should conform the RHTT sample's gauge during the test process for a uniaxial tensile stress and strain paths. The foremost criteria that obviously should be fulfilled for the RHTT sample's gauge are the strain and the stress states associated to the uniaxial tensile test. Besides, we introduced others criteria, to add more constraints on the shape optimization problem. Such criteria are the stress triaxiality (Σ) (Gruben et al., 2011) and Lode parameter (L) (Dunand and Mohr, 2014). Table 2 presents the target output values, the strain and stress ratio paths, the stress triaxiality and Lode parameter that should conform a uniaxial tensile test for isotropic material behaviour.

To extract the optimal set of design variables, the desirability function approach, disseminated by Derringer and Suich (1980), was used. This method is a useful technique for the optimization of multiple responses y_i (target outputs) by maximizing a composite desirability function that maximizes the desirability of each output response (the individual desirability functions). The general approach is to first transform each response y_i into an individual desirability function $d_i$that varies over the range$0 \le d_i \le 1$.

The composite or overall desirability is given in Eq. (1) and can be defined as the geometric mean of each individual desirability d_i's (i = 1,2, …,n).

$$D = (d_1.d_2.....d_n)^{\frac{1}{n}} \tag{1}$$

Eq. (1) can be extended to a general form given in Eq. (2),

$$D = \left(d_1^{w_1}.d_2^{w_2}....d_n^{w_n}\right)^{\left(\frac{1}{\sum^{w_i}}\right)} \tag{2}$$

where the w_i refers to the weights, which satisfy the following relation $\sum_{i=1}^{n} w_i = 1$and that the w_i can be tuned to favorite some possible responses over others less significant.

Table 3
Boundaries of design variables.

Design variables	l (mm)	w (mm)	r (mm)
Lower bound	12	3	6
Upper bound	24	6	8

Table 4
Full factorial design of experiments for the RHTT finite element simulation.

N° of Run	l	w	r	specimen reference
1	12	3	6	*l12w3r6*
2	24	3	6	*l24w3r6*
3	12	6	6	*l12w6r6*
4	24	6	6	*l24w6r6*
5	12	3	8	*l12w3r8*
6	24	3	8	*l24w3r8*
7	12	6	8	*l12w6r8*
8	24	6	8	*l24w6r8*

Table 5
Design of experiment matrix and the obtained target outputs.

Specimen reference	Strain ratio$\rho = \varepsilon_{zz}/\varepsilon_{\theta\theta}$	Stress ratio $x = \sigma_{zz}/\sigma_{\theta\theta}$	Triaxiality Σ	Lode L
l12w3r6	−0.491	0.003	0.331	−0.979
l24w3r6	−0.492	0.005	0.332	−0.977
l12w6r6	−0.476	0.017	0.338	−0.952
l24w6r6	−0.475	0.022	0.341	−0.942
l12w3r8	−0.482	0.005	0.332	−0.976
l24w3r8	−0.492	0.006	0.333	−0.973
l12w6r8	−0.482	0.021	0.340	−0.943
l24w6r8	−0.487	0.031	0.344	−0.924

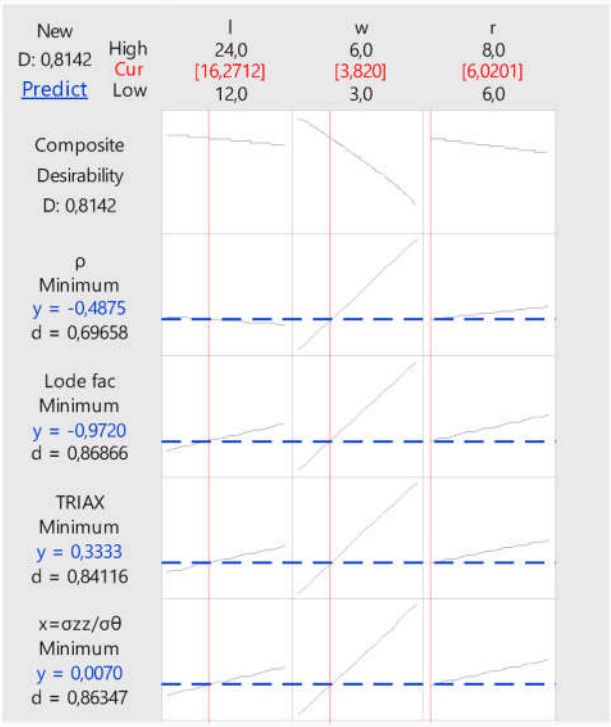

Fig. 4. Desirability function approach applied in the optimization of multiple responses.

Eq. (3) represents the two-sided desirability function, or the so-called Nominal-The-Best (NTB), when the target response y_i is set between the lower bound (L) and upper bound (U) and expected to achieve a particular target value (T). The α_1 and α_2 refer to the shape constants of the individual desirability functions, that allow the practitioners to specify the shape of d_i . In case of linear desirability, the α_i values are set equal to unity.

$$d_i = \begin{cases} 0 & y_i < L \\ \left(\dfrac{y_i - L}{T - L}\right)^{\alpha_1} & L \le y_i < T \\ \left(\dfrac{U - y_i}{U - T}\right)^{\alpha_2} & T < y_i \le U \\ 0 & y_i > U \end{cases} \tag{3}$$

The optimization of multiple responses is conducted using "Response Optimizer" tool of Minitab statistical software, which is a solver using desirability method for the optimization problem formulated by RSM method (Kalmegh and Khodke, 2018; Islam and Haghshenas, 2019). The optimal set of the design variables (*l,w,r*) is obtained based on the composite desirability D function approach, (i.e., a global desirability function), to simultaneously optimizes multiple responses process. As much as the composite desirability D is closer to unity, as higher satisfaction of target values is obtained.

The design variables' space is chosen in the ranges presented in Table 3. The design variable boundaries are based on several proposed RHTT sample geometries cited in the literature (e.g. see Table 1) and preliminary FE simulations. Table 4 presents a full factorial design of experiment that represents eight finite element simulation runs of RHTT.

3.1. Surrogate model for shape optimization

A full factorial design of experiment (DoE) is composed of 8 runs. This choice is adopted to guarantee that all the possible combinations are achieved. Table 5 lists the DoE matrix and the results of the 8 FE simulations. The analysis of these findings shows the multiple results, which are somehow close to the target outputs that satisfy the uniaxial tensile state; however, it is necessary to push the optimization for better-optimized design variables. In addition, it seems that sensitivity analysis of the different design variables on the response of the RHTT could be useful in order to tune the weighting coefficients to higher values for the most sensitive design variables during the optimization process.

The Analysis of Variance (ANOVA) is a statistical method, which is used to analyse the effect of the design variables (l, w, r) on the output parameters(x, ρ, Σ, L), and then to rank the design variable sensitivity of the ring specimen's shape based on the RHTT response. The relevance level of the design variable refers to the statistical p-value. The p-value in this case is at the 5% level of significance (95% confidence level). If p-value is less than 0.05, it indicates that the power level has a statistically significant effect on the responses (Sarikaya and Güllü, 2014; Prasad and Babu, 2017). Seeking for simplicity for the paper presentation, the ANOVA tables for regression analysis of the stress ratio (x), the strain ratio (ρ), the stress triaxiality (Σ) and the Lode parameter (L) target outputs are listed in Table B1 in Appendix B. One can observe from this table that the p-value corresponding to the design variable w (width of the specimen's gauge section) has the lower p-value and is less than 0.05 for all the ANOVA analysis. This means that the width of the specimen's gauge section is the higher significant design variable that affects the target outputs, as also confirmed by the percentage contribution of p, as shown in Table B1.

A linear regression model is constructed using RSM, as a first attempt to relate the design variables (l, w, r) to the target outputs (x, ρ, Σ, L), in order to determine the optimal design variables, for which a best approximation of the imposed target values is obtained. The linear regression equations are given in the system of equations (Eq. (4)).

To assess the global fit of the model presented in the regression

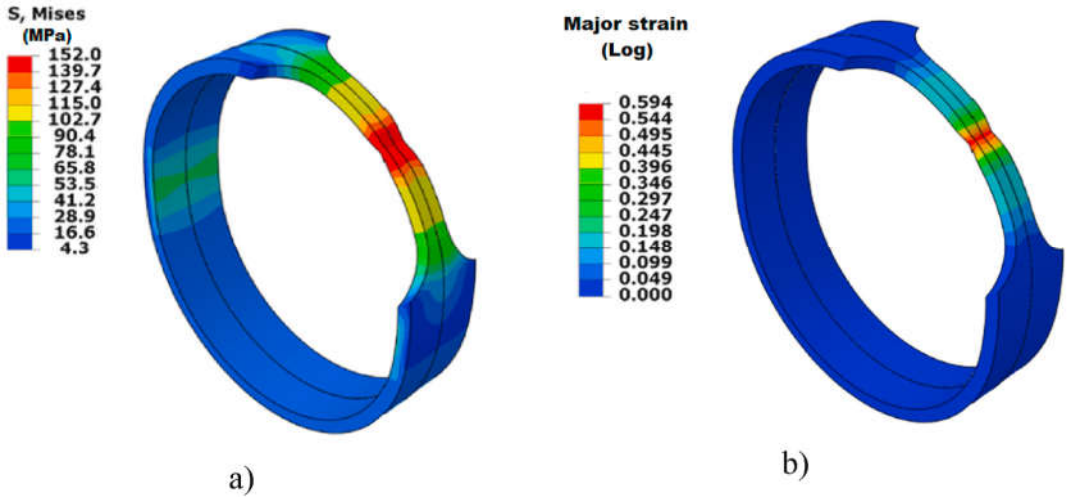

Fig. 5. Simulation of the RHTT using the optimized design variables ($l = 16.3$ mm, $w = 3.8$ mm; $r = 6.0$ mm).Within the ring specimen centre gauge almost at the onset of necking: a) von Mises equivalent stress distribution; b) the hoop strain distribution (major logarithmic strain).

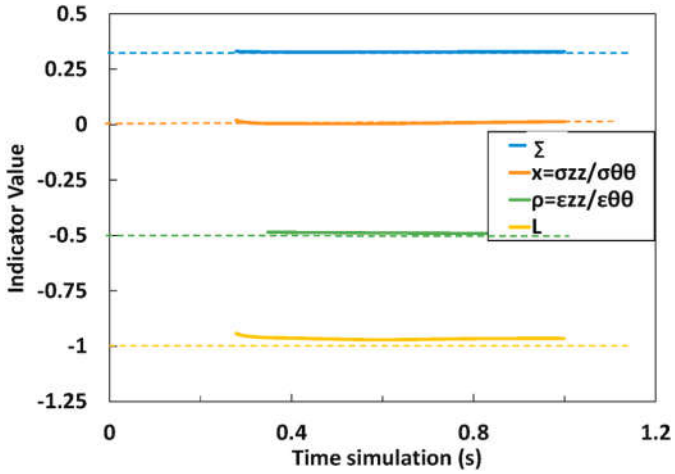

Fig. 6. Evolution of the indicators (target output values) calculated using FE simulation of the shape optimized RHTT sample. The stress and strain distribution, within the specimen along the hoop direction, matchs the theoretical target values (see, Table 2) defining the uniaxial tensile state.

equations, the regression statistical value R-sq is calculated for the target outputs: stress ratio (x), strain ratio (ρ), stress triaxiality (Σ) and Lode parameter (L). They are equal to the following values: 99.56%, 99.80%, 99.64% and 99.73%, respectively. This shows that the statistical correlation coefficient is greater than 0.99 for all the target outputs. Moreover, no curvature was noticed in the responses in the region of interest of design variables (ranges of design variables); then linear RSM is accurate enough to approximate the model response. Thus, the constructed regression model has demonstrated a real effectiveness to match the imposed target outputs, which in return contribute to gain optimal design variables that ensure the uniaxial tensile stress and strain states.

Since the design variable w has the most significance effect (e.g. see, Table B1 in Appendix B); thus, we have tuned the corresponding weighting coefficient to improve the convergence toward a higher composite desirability D close to 1. It should be mentioned that individual desirability must be also greater than 0.7 (i.e. 70%), which indicates that the obtained value is satisfactory (Zaddem, 2014).

3.2. Optimal shape of the RHTT sample

Using the desirability function approach (see, Fig. 4), the optimal design variables for the RHTT sample's shape are as follows: $l = 16.27$ mm, $w = 3.82$ mm and $r = 6.02$ mm. The obtained individual desirability attained narrowly their target values ($y_i \simeq T_i$) as defined in Table 2, with also a satisfactory high composite desirability D value, which is equal to 0.8142 (81.42%).

Finally, the set of the design variables for the RHTT specimen's shape, which are adopted for machining the experimental sample and building the numerical model are as follows: $l = 16.3$ mm, $w = 3.8$ mm; $r = 6.0$ mm.

The finite element (FE) model of the optimal ring specimen was carried out and obtained results are presented in Fig. 5. In this simulation, we show the equivalent stress and major strain, which were postponed until the appearance of a small mesh distortion, where it is revealed strain localization in the gauge section centre of RHTT specimen. The distribution of von Mises equivalent stress and the major hoop strain within the gauge section are displayed in Fig. 5a and b, respectively. A homogeneous distribution of stress and strain was obtained. Fig. 6 shows that the indicators (x,ρ, Σ and L), calculated from FE simulation of the optimized RHTT match with the uniaxial stress state and properly attain the target output values (theoretical values). This corroborates that the optimized sample is the suitable specimen to carry out the RHTT.

$$\begin{cases} x = 0.0171 - 0.001156\,l - 0.00273\,w - 0.00320\,r + 0.000186\,lw + 0.000101\,lr + 0.000776\,wr \\ \rho = -0.58964 + 0.001448\,l + 0.01784\,w + 0.01467\,r + 0.000077\,lw - 0.000304\,lr - 0.002299\,wr \\ \Sigma = 0.3294 - 0.000173l - 0.00053w - 0.00096r + 0.000077lw + 0.000031\ lr + 0.000289wr \\ L = -0.9757 - 0.000867\,l - 0.00576w - 0.00306r + 0.000356lw + 0.000198\ lr + 0.001636\,wr \end{cases} \quad (4)$$

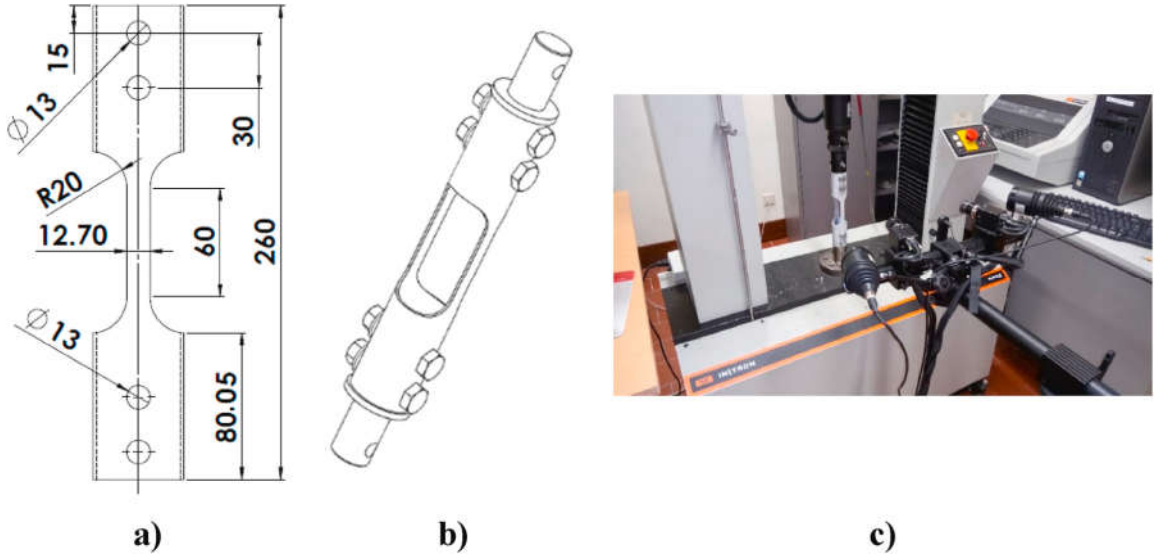

Fig. 7. Tubular axial tensile test specimen: a) Engineering drawings and dimensions of the tubular axial tensile test specimen; b) 3D drawing sketch of the sample with specific mandrels to tie it to the tensile machine jaws; c) experimental setup used to carry out uniaxial tensile test along the tube axial direction.

Table 6
Set of parameters used for strain measurement using GOM ARAMIS 5 M Stereo Digital Image Correlation system.

DIC Analysis Parameters	
Camera Manufacturer	Not Specified – Part of the package
•Lens Manufacturer	Schneider
•Lens Focal Length	23 mm
•FOV	175 × 130 mm
•Stereo-Angle	25°
•SOD	630 mm
•Image Acquisition Rate	1 s
•Patterning Technique	Black spackle pattern applied over matt white pre-painted surface, using Lack Spray
•Approximate Pattern Feature Size	<0.2 mm (optical microscopy aided by generic measurement software)
DIC Hardware Parameters	
Software Package	GOM Cohen et al., 1998
•Subset Size	11 pixels
•Step Size	5 pixels
•Subset Shape Function	affine
•Strain Formulation	Logarithmic

It is worth pointing out the significance of the width (w) of the gauge area of the ring specimen on the stress state for the uniaxial tensile test. In this case, the gauge length (l) has less effect on the stress state, as it has been demonstrated referring to ANOVA (see, Table B1). On the other hand, the (l/w) ratio should be also taken larger than the value of 4 (Wang et al., 2002) in accordance with recommendation of the ASTM E−8 standard, in order to meet the strain and stress distribution state corresponding to the uniaxial tensile test. However, the initial ring diameter bounded the larger possible length of the gauge section of the ring specimen, which in turn influences the determination of the sample width. Accordingly, depending of the initial ring diameter, particularly for small initial diameter tubes, the proposed methodology is recommended to optimize the ring specimen, which undergoes the stress and strain distribution of uniaxial tensile state. In this study, the final ring specimen geometry has a length to width ratio (l/w) equal to 4.34. The ratio of the radii of fillet under the width of gauge section (r/w) is equal to = 1.58, which is in concordance with the results obtained by Arsene and Bai (1996).

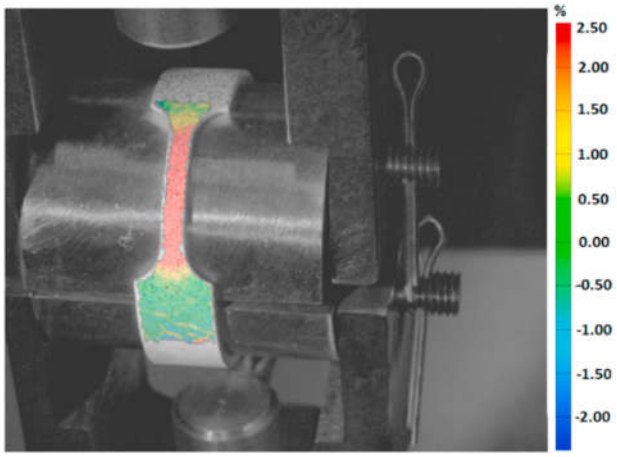

Fig. 8. Ring hoop tensile test specimen mounted on the RHTT test fixture tool and displaying the contours of the measured major strain field (strain percentage) using stereo DIC technique.

4. Experimental details

The as-received AA6063-T6 aluminium alloy has a high tensile strength due to heat treatment (T6). In order to increase its ductility and to achieve enhanced formability, an annealing treatment was carried out. The specimens were fully annealed at (O) state using a thermo scientific carbolite furnace (Model number 3216). The annealing process was performed by heating all specimens at 420 °C and maintaining them at this temperature for 3 h, and then a controlled cooling rate of 0.5 °C/mn is achieved up to the temperature of 260 °C. To prevent any kind of ageing of the aluminum alloy that can affect the measured mechanical properties. The whole specimens were tested within maximum 4 days after their annealing process.

4.1. Tensile test along axial direction

The uniaxial tensile samples along axial direction were obtained by cutting out a curved dog-bone specimen of the tube using Electrical Discharge Machining (EDM) technique. Fig. 7 shows the engineering drawing of the uniaxial tensile specimen and the geometrical

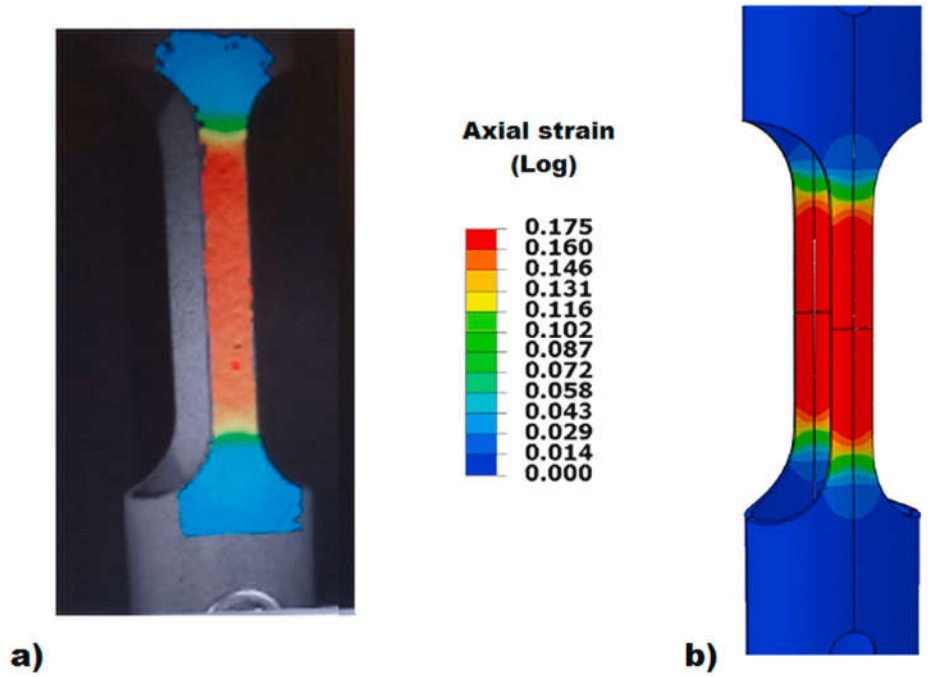

Fig. 9. Uniaxial tensile test along the tube axial direction: a) experimental axial strain; b) numerical axial strain.

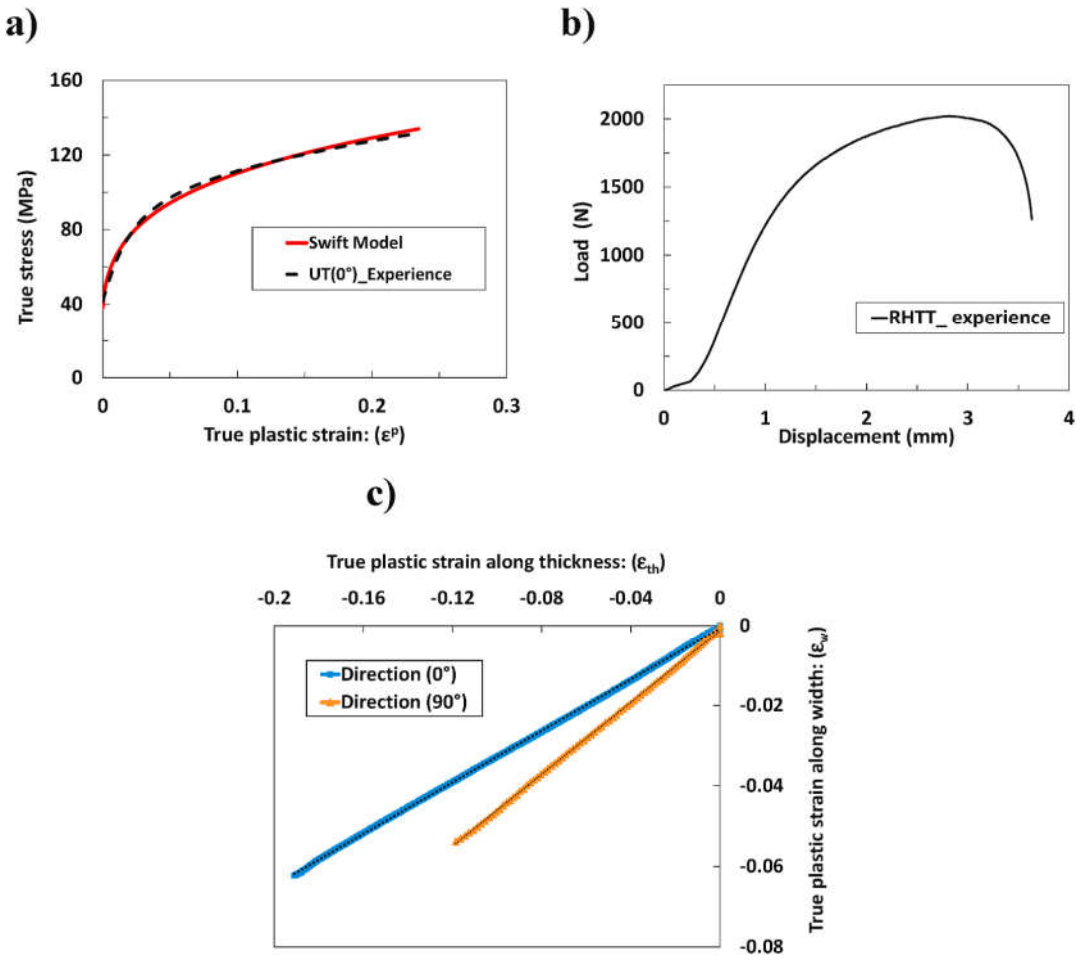

Fig. 10. a) True stress-strain curve along the tube axial direction; b) Load – displacement curve of the RHTT (average curve obtained from six experimental responses); c) Determination of the experimental Lankford coefficients along axial (0°) and hoop (90°) directions.

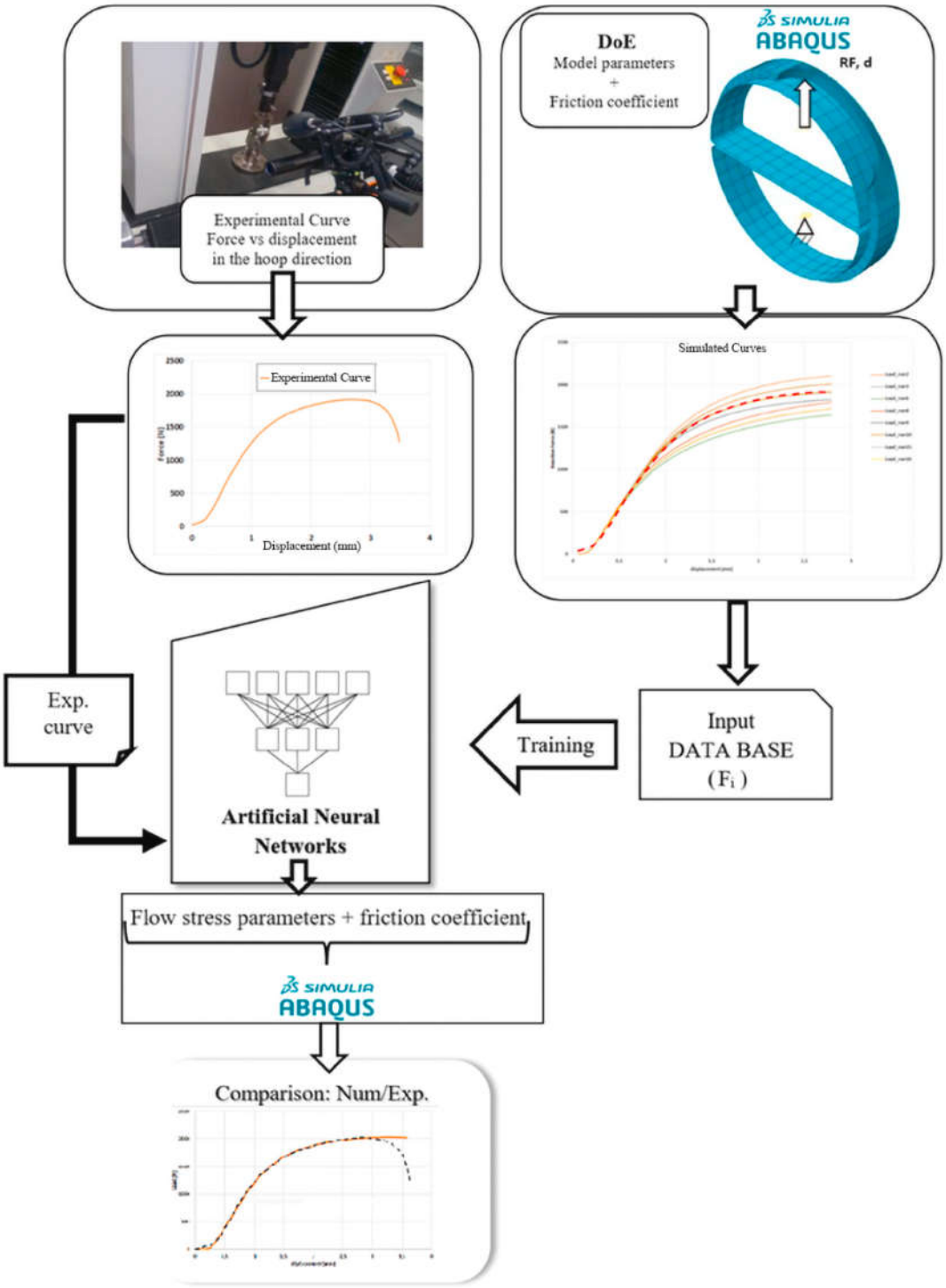

Fig. 11. Flow chart of the inverse analysis using a hybridization of RHTT experimental results with FEM simulation and ANN model to identify simultaneously the actual flow stress parameters along the hoop direction of the tubular material and the friction coefficient between the sample and the D-shaped block tool interface.

dimensions for this specimen (see, Fig. 7a). The advantage of this cutting method is to obtain accurate sample dimensions and to avoid any induced residual stresses that may occur within the sample when using the conventional machining process. This can assure and conserve the initial mechanical properties of the tested tubular material. Fig. 7b shows the design drawing of the specific mandrels, which were manufactured to tie the sample to the tensile machine jaws. Afore tensile testing, the specimens were prepared by applying a random black speckle pattern, over a previous mat white paint applied on the specimen surface to enable strain measurement using GOM ARAMIS 5 M Stereo Digital Image Correlation, (DIC) system. This system has a strong industrial vocation all the procedures and definitions are well defined in the equipment's manual (ARAMIS, 2009). The information about DIC procedures used in this work during the tests performed are shown in the Table 6.

Tensile tests were conducted at stroke rate of 5 mm/min, using an INSTRON 4206 universal tensile-testing machine of capacity of 100 tones. Fig. 7c shows the experimental setup used to carry out uniaxial tensile test along tube's axial direction.

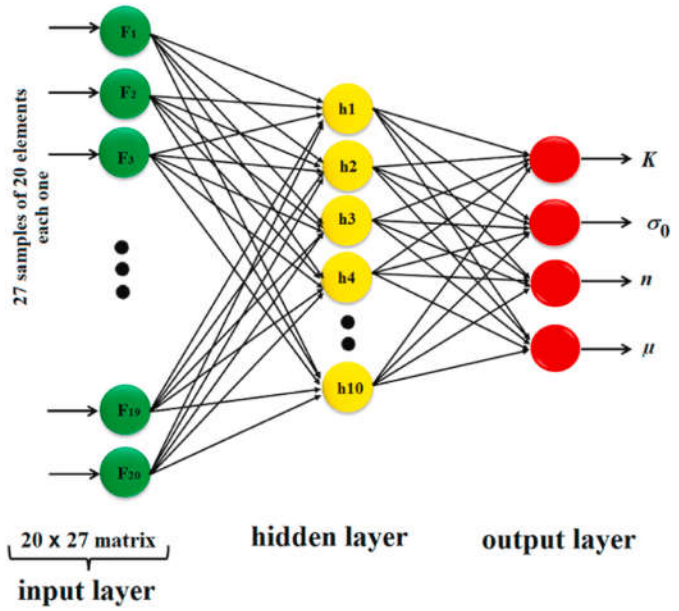

Fig. 12. The artificial neural network feed forward architecture used to identify the flow stress curve in the hoop direction along with the friction coefficient; where the force curves are supplied simultaneously to ANN as 27 training datasets that contained 20 data points in every curve [20 x 27] matrix or points representing for each point, the force increment.

4.2. Ring hoop tensile test (RHTT)

Fig. 8 shows the test fixture tool used to mount the ring sample on the tensile machine and to carry out the RHTT on the optimized specimens. This test fixture tool consists of an upper and lower clevis to be tied to the tensile machine jaws, D-shaped blocks and clevis pins. The ring specimens were machined according to the optimal design variables (*l, w,r*) and using the cutting (EDM) technique. Then, a random black speckle pattern is applied on the ring specimen to be able to measure strains using stereo DIC system. The ring's outer nominal diameter is 50 mm and nominal thickness of 2 mm. The displacement rate of the actuator was set to 5 mm/min.

In order to reduce the effect of the friction between the inner specimen's surface and the D-shaped blocks on the RHTT force-displacement results, two layers of PTFE lubricant and oil were applied. The centre of the gauge section of the ring specimen is positioned on the D-shaped block at an angle of 45° according to vertical direction in order to avoid the bending effect and to attempt to localize the necking then fracture in the specimen's gauge centre.

4.3. Experimental results

Fig. 9a shows the experimental strain field within the specimen's gauge section of the uniaxial tensile test along the tube axial direction. Fig. 9b depicts the numerical simulation for the similar experimental test conditions. It is clear to observe in Fig. 9, that the proposed sample undergoes a uniaxial tensile test along the tube axial direction. Then mechanical properties of the tubular material, along the axial direction, are inferred using this test.

Fig. 10a shows the true stress – true strain curve obtained for the AA6063 –O aluminium alloy along the tube axial direction. The Swift power-type strain hardening law is a proper model for fitting the experimental data. The fitted Swift strain hardening parameters are as follows:$K = 186.6$ MPa, $\sigma_0 = 38.0$ MPa and $n = 0.23$. Fig. 10b represents the experimental responses of the RHTT obtained using the optimized ring hoop specimen. This curve represents a statistical average response obtained from six experimental results for RHTT.

Table 7
Design ranges of the material parameters and the friction coefficient used to run FE simulation of the ring hoop tensile test.

Variables	Lower bound	Midpoint	Upper bound
Strength coefficient K (MPa)	150.0	200.0	250.0
Pre-strain ε_0	5.10^{-4}	$7.5.10^{-4}$	10^{-3}
Yield stress σ_0(MPa)	40.0	50.0	60.0
Strain hardening exponent n	0.100	0.175	0.250
Friction coefficient μ	0.08	0.12	0.16

Fig. 10c shows the plots of experimental thickness strain *versus* width strain obtained from the uniaxial tensile test in the axial direction and along hoop direction from the RHTT. It depicts two straight lines, where the slope of each one represents the experimental Lankford coefficient in the tube axial and hoop directions. Analysing these results, one can conclude that the tubular material presents the anisotropic behaviour of strains. The measured Lankford coefficients are $r_0 = 0.322$ and $r_{90} = 0.485$, where the (0°) and (90°) refer to the axial and hoop directions of the tubular material, respectively.

5. Inverse identification of material parameters along hoop direction

The chief aim of the present investigation is to accurately identify the actual flow stress curve along the ring hoop direction using the optimized RHTT sample. Despite the strain and stress paths for uniaxial tensile test are satisfied during RHTT, the identified material parameters are vitiated by errors originated from the presence of friction due to the contact between the ring specimen and the D-shaped blocks (tool). Thus, the experimental force –displacement curve (i.e. raw response obtained from RHTT) is a degenerate response of the mechanical material behaviour, since the friction effect alters the deduction of the actual flow stress curve. In this context, we proposed an efficient method that uses the experimental global response: the force –displacement curve recorded during RHTT and isolates the flow stress curve along the hoop direction from the effect of friction coefficient on the measured response. The proposed method is an inverse identification analysis based on the hybrid approach that combines experimental results, FE simulations and artificial neural network model (ANN). Fig. 11 displays the flow chart, which illustrates the proposed inverse analysis procedure to identify simultaneously the flow stress curve and the friction coefficient.

ANN is one of the supervised machine learning (ML) algorithms. The performance of this algorithm is based on learning using training process from data confined in inputs and outputs. This allows to build an approximate functional dependency between inputs and outputs. In this work, the constructed artificial neural network (ANN) model is used to identify by inverse analysis approach the set of the unknown parameters (i.e. material parameters and friction coefficient) from the experimental RHTT response. This ANN model maps the global force-displacement curve of the RHTT and the flow stress curve of the tubular material along with the friction coefficient. The architecture of the artificial neural network (ANN) is shown in Fig. 12.

In this work, the built ANN is a feed-forward network three layers: (input, hidden and output layers). The Log-sigmoid (Logsig) and linear (Purelin) function are used as activation functions in the hidden and output layer in MATLAB Neural Network Toolbox™ 7 (MATLAB, 2010). The training sets use backpropagation with Levenberg-Marquardt (LM) algorithm to update and determine weights and biases of the neurons of the ANN model.

It is worth noting that the number of neurons in the hidden layer of the ANN model and the learning rate of the network have a substantive effect on the performance of the ANN. The number of the adequate

Table 8
The parameters used to define the ANN model.

Type	Feed-forward network
Learning system	Supervised learning
Training function	Levenberg-Marquardt back-propagation
Activation functions	Log sigmoid (Logsig) Linear (Purelin)
Number of layers	3 layers (input: hidden: output), (20x27):10:4
Number of hidden neurons	10
Learning rate	0.01
Performance function	Mean squared error (MSE)

neurons in the hidden layer is 10 and the learning rate of the network is 0.01. These values were determined by trial and error method and they were found sufficient for the best performance of the ANN model.

The strain-hardening behaviour is supposed to obey to the Swift law (K, ε_0 and n) and the friction is characterized by Coulomb friction coefficientμ. The chosen ranges of the material parameters and friction coefficient, as listed in Table 7, are based on preliminary RHTT finite element simulations and prior experiences, for which the experimental response is located in the range of the generated RHTT results. However, if the identified parameters are found to reach any of the boundary of the defined variable space, it is checked and the range is adjusted.

The design matrix listed in Table A.1 (Appendix A.) is used to generate the FE simulation database of RHTTs. The design of experiment of Box-Behnken method (Box and Behnken, 1960) is applied to obtain the different combination of parameters. The generated dataset is composed of 27 force –displacement curves. The ANN input datasets are the force values that correspond to total displacement of 2.6 mm, which is graduated into equi-spaced intervals (2.6 mm was equally divided to obtain 20 displacement increments). Thus, linear interpolation is used to calculate for all the forces, obtained by FE simulation, in the same values of displacement graduation. Each force curve is then constituted of a 20 data points. The 27 force curves (27 samples) were introduced simultaneously to the network as a matrix [20x27]. Prior to the introduction, the input and output datasets were normalized with linear transformation. This will help in effective faster training as well as reducing the chances during training to get trapped in local minima and therefore, avoid of getting multiple solutions for the inverse problem solved by ANN.

It is worth noting, that using limited training dataset for ANN model is challenging for obtaining effective network. However, it is possible to accurately train ANN models with limited dataset using either Bayesian regularization (Burden and Winkler, 2008) or early stopping method to avoid the problem of ANN overfitting. The gain of using Bayesian regularization is that it does not need for further validation subset. However, its drawback is that it requires more computation time. As an alternative, the commonly early stopping method is used in this work to avoid overfitting of the network during the training process. Indeed, these input datasets were randomly distributed into three subsets: the training, validation and testing subsets, respectively, for learning the ANN model, for the generalization capacity and for assessing its performance for unknown data. The input dataset is randomly partitioned into 70% for training, 15% for validation, and 15% for testing. The error on the validation set is controlled during the training process. The training stops automatically as validation error starts by increasing instead of continuous decreasing of the validation data mean square error (MSE).

To test the performance and assure the effectiveness of network learning, additional virtual responses were randomly generated using finite element model, for which the parameters were known and in the ranges of the considered parameters, and then we used them as a virtual experimental input curve in the trained network, assuming that the corresponding parameters were unknown. This is an effective way to check again the performance capacity of the built network by using extra input datasets that are unknown for the trained ANN model, thus avoiding multiple solutions for the inverse problem. The details of the used network are given in Table 8.

Fig. 13a shows that the best validation performance of the network was obtained after 80 epochs, i.e., this is the optimal number of sweeps (forward and backward passes) of the entire dataset through the ANN algorithm that has been completed (training, testing and validation). The training is stopped automatically at this point using the most frequently regularization technique (early stopping method) for networks to avoid overfitting, and thus results in a robust network performance to predict accurate outputs from unknown inputs. The validation

Table 9
Identified material parameters along with the friction coefficient using the built ANN model.

Strength coefficient K (MPa)	Yield stressσ_0 (MPa)	Strain hardening exponent n (−)	Friction coefficient μ (−)
223.4	43.0	0.231	0.111

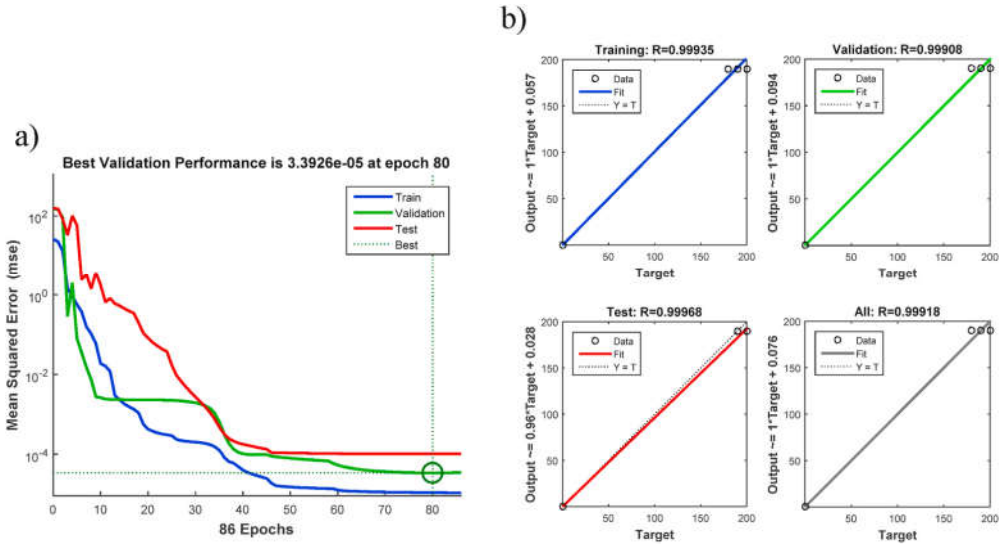

Fig. 13. Best validation performance of network: a) The performance test shows good generalization competence of the constructed ANN model; b) The linear regression analysis assesses the correlation between targets and actual ANN outputs.

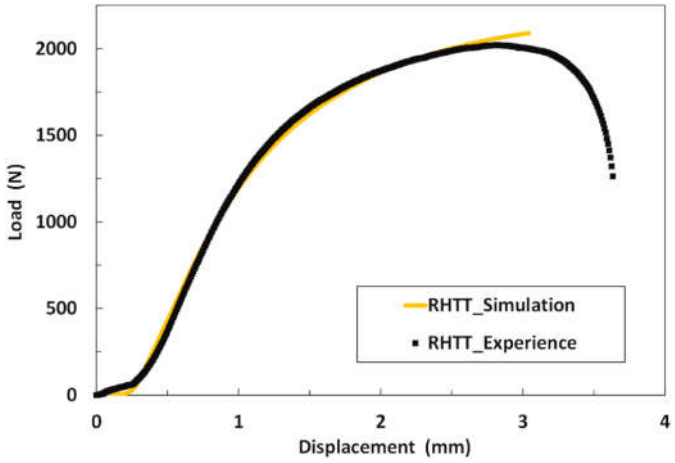

Fig. 14. Comparison between experimental and numerical curves of the RHTT. The finite element simulation of the RHTT response is obtained using the identified material parameters and the friction coefficient, as given in Table 9.

curve reaches the best validation performance for mean squared error (MSE) equal to $3.392.10^{-5}$at 80 epochs and the test curve has an MSE value of about 10^{-4}.

Fig. 13b shows the coefficients of linear regression of the training, validation and testing during the learning process of the network. The R-plots represent regression analysis and the correlation between the target and the actual ANN outputs. The obtained correlation coefficient (R) value is 0.999 (closer to 1) and then a minimum value of the mean square error (MSE) is achieved, which indicates the performance of the constructed ANN model.

Afterwards, the experimental RHTT force curve given in Fig. 10b is used as input dataset (20 experimental points) in the ANN model to predict simultaneously, the strain hardening parameters and the friction coefficient. The obtained results are listed in Table 9.

6. Verification of the proposed methodology

Using the identified parameters for the flow stress curve along the hoop direction of the AA6063-O aluminium alloy, given in Table 9, the FE simulation of RHTT was carried out, and compared to experimental curve (i.e. Fig. 10b: force – displacement curve). Fig. 14 displays the comparison between RHTT simulated curve and experimental one. One can observe the good agreement between the two results. In addition, Fig. 15 shows the measured major strain (measured hoop strain using stereo DIC system) within the gauge section of the optimized RHTT specimen and the major strain calculated by FE simulation. It is clear that the simulated major hoop strain accurately matches the measured one. Moreover, it is ascertained for the experimental and numerical RHTT, that the sample necking was indeed occurred at almost the same location, and for practically the same strain value. This agreement could be attributed to the accurate and effective determination of the friction coefficient, which probably can alter the position of the necking and the obtained distribution of the resulted strain distribution.

Fig. 16 depicts the main results obtained, validates the proposed approach and illustrates the comparison between the experimental and the predicted results. Based on these findings, it is clearly demonstrated that the experimental true stress – true strain obtained using stereo DIC system, (black dashed curve) is in good agreement with the simulated RHTT curve, which is obtained using the input parameters given in Table 9 and identified by the inverse identification method (coupling experiments, FEM- ANN). It is of paramount importance to mention, that this curve is a degenerated response of the material behaviour, since it is altered with the effect of the friction coefficient. Indeed, the effective flow stress curve along the hoop direction is plotted using the strain hardening parameters:$K = 223.4$ MPa,$\sigma_0 = 43.0$ MPa and $n = 0.231$, as analytical function of the true plastic strain (yellow solid line). In addition, the red coloured curve (red solid line) corresponds to the proper flow stress along the hoop direction, which is calculated using the Hill'48 yield criterion. In this context, the experimental anisotropy r-values r_0,r_{90} and the strain-hardening curve (red dotted line) along the tubular axial direction (reference direction 0°) are used to model the material behaviour undergoing a uniaxial tensile test along the hoop direction (90°). In this plot, it is clearly exposed the good agreement between both curves. Accordingly, one can conclude that the proposed method is suitable to correctly identify simultaneously the flow stress parameters and the friction coefficient between the RHTT sample and the D-shaped blocks.

7. Conclusion

In the first part of this study, shape optimization method is proposed to obtain the accurate design dimensions of the RHTT specimen that catches the stress-strain distribution of uniaxial tensile. This method is based on surrogate modelling that uses (DoE) and finite element method to construct an approximated model, which defines the relationship between design variables and target outputs using response surface methodology (RSM). The shape optimization problem is formulated as a

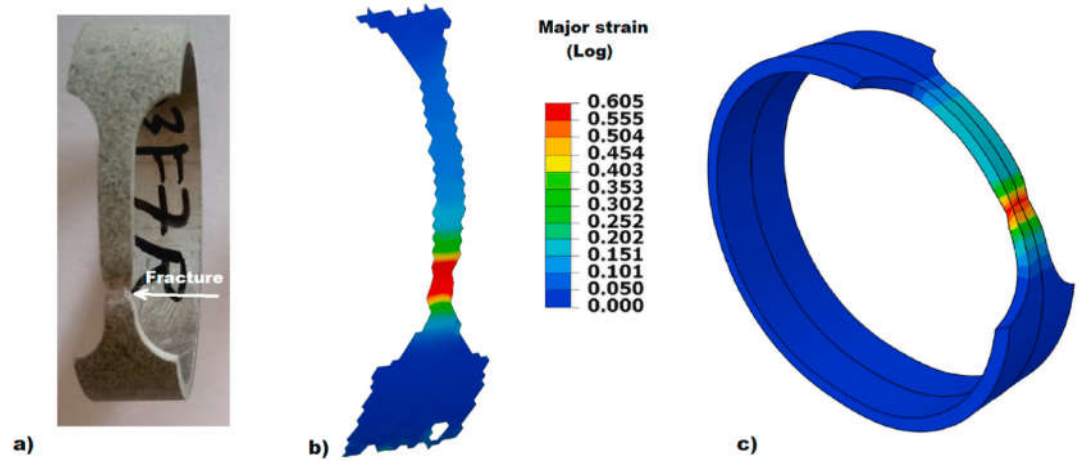

Fig. 15. Comparison between the experimental and numerical results obtained using the optimized RHTT specimen for the assessment of the proposed methodology: a) experimental RHTT specimen deformed at fracture; b) experimental major strain along ring hoop direction measured using stereo DIC system; c) simulation of the major strain (hoop strain) using FEM model.

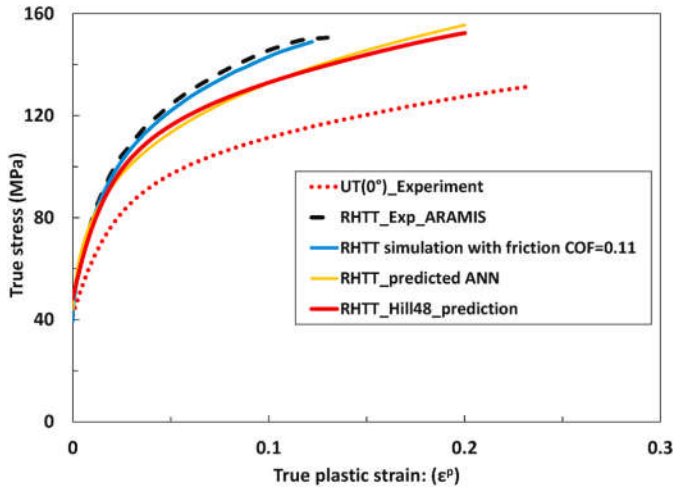

Fig. 16. Comparison between experimental and predicted flow stress curves and the discrepancy between effective stress-strain curve along the ring hoop direction and the curve integrating the material behaviour along with the effect of the friction coefficient. The Hill48 yield criterion was used for modelling the material behaviour and good agreement was obtained between ANN and the Hill48 predictions.

multiple response problem optimization, solved using the desirability method. Moreover, ANOVA was accomplished to determine the most significant geometrical design variables, and then guides the user to tune the weighting coefficients, which take account of more sensitive variables to increase desirability during the multiple response optimization process.

The second part of this study is to experiment the designed RHTT specimen in order to identify accurately the effective flow stress curve of the tubular material along the hoop direction. An inverse identification procedure based on hybrid methodology using (DoE), finite element analysis and ANN model, is proposed and applied. This approach's advantage is the decoupling of the flow stress curve and the effect of the friction (between the RHTT sample and the D-shaped block) from the global degenerate RHTT force response, which represents an intermixture effects of the material properties and the friction coefficient. The validation results corroborate the abovementioned statements.

CRediT authorship contribution statement

Zied Ktari: Investigation, Software, Data curation, Formal analysis, Writing - original draft, Writing - review & editing. **Carlos Leitão:** Experimental validation, Investigation, Formal analysis, Writing - review & editing. **Pedro A. Prates:** Writing - review & editing, Validation. **Ali Khalfallah:** Conceptualization, Methodology, Writing - review & editing, Resources, Supervision.

Declaration of competing interest

The authors declare that they have no known competing financial interests or personal relationships that could have appeared to influence the work reported in this paper.

Acknowledgement

This work was supported by the Portuguese Foundation for Science and Technology and by FEDER funds through projects with references UID/EMS/00285/2013 (Research Unit project) and POCI-01-0145-FEDER-031243 (RDFORMING project, via program PT2020).

Appendix A

Table A.1
Design matrix using DoE of Box-Behnken method for finite element simulation runs of RHTT

N° of run	K(MPa)	σ_0(MPa)	n	μ
1	150.0	40.0	0.175	0.12
2	250.0	40.0	0.175	0.12
3	150.0	60.0	0.175	0.12
4	250.0	60.0	0.175	0.12
5	200.0	50.0	0.100	0.08
6	200.0	50.0	0.25	0.08
7	200.0	50.0	0.100	0.16
8	200.0	50.0	0.250	0.16
9	150.0	50.0	0.175	0.08
10	250.0	50.0	0.175	0.08
11	150.0	50.0	0.175	0.16
12	250.0	50.0	0.175	0.16
13	200.0	40.0	0.100	0.12
14	200.0	60.0	0.100	0.12
15	200.0	40.0	0.250	0.12
16	200.0	60.0	0.250	0.12
17	150.0	50.0	0.100	0.12
18	250.0	50.0	0.100	0.12
19	150.0	50.0	0.250	0.12
20	250.0	50.0	0.250	0.12
21	200.0	40.0	0.175	0.08
22	200.0	60.0	0.175	0.08
23	200.0	40.0	0.175	0.16
24	200.0	60.0	0.175	0.16
25	200.0	50.0	0.175	0.12
26	200.0	50.0	0.175	0.12
27	200.0	50.0	0.175	0.12

Appendix B

Table B.1
Analysis of Variance (ANOVA) for the target outputs: stress ratio (x), strain ratio(ρ), stress triaxiality(Σ) and Lode parameter (L).

Analysis of Variance (ANOVA) of the stress ratio (x).

Variance source	DF	Sum of squares (SS)	Mean squares (MS)	F-Value	p-Value	% contribution of p
Model	6	0.000774	0.000154	48.63	0.124	99.614
l	1	0.000043	0.000043	12.64	0.175	5.534
w	**1**	0.000659	0.000659	193.58	**0.046**	84.813
r	1	0.000036	0.000036	10.46	0.191	4.633
*l*w*	1	0.000022	0.000022	7.05	0.117	2.831
*l*r*	1	0.000003	0.000003	0.86	0.524	0.386
*w*r*	1	0.000011	0.000011	3.42	0.206	1.416
Error	1	0.000006	0.000003			0.386
Total	7	0.000777				100

Analysis of Variance (ANOVA) of the strain ratio (ρ).

Variance source	DF	Sum of squares (SS)	Mean squares (MS)	F-Value	p-Value	% contribution of p
Model	6	0.000344	0.000057	81.25	0.085	100
l	1	0.000032	0.000032	45.30	0.094	9.302
w	**1**	0.000176	0.000176	**249.15**	**0.040**	51.163
r	1	0.000011	0.000011	14.96	0.161	3.197
*l*w*	1	0.000004	0.000004	5.41	0.258	1.163
*l*r*	1	0.000027	0.000027	37.71	0.103	7.849
*w*r*	1	0.000095	0.000095	134.96	0.055	27.616
Error	1	0.000001	0.000001			0.291
Total	7	0.000344				100

Analysis of Variance (ANOVA) of stress triaxiality (Σ)

Variance source	DF	Sum of squares (SS)	Mean squares (MS)	F-Value	p-Value	% contribution of p
Model	6	0.000170	0.000028	46.71	0.112	100
l	1	0.000009	0.000009	14.10	0.166	5.294
w	1	0.000149	0.000149	246.01	**0.041**	87.647
r	1	0.000007	0.000007	10.89	0.187	4.117
*l*w*	1	0.000004	0.000004	6.30	0.241	2.353
*l*r*	1	0.000000	0.000000	0.47	0.618	0
*w*r*	1	0.000002	0.000002	2.48	0.360	1.176
Error	1	0.000001	0.000001			0.588
Total	7	0.000170				100

Analysis of Variance (ANOVA) of Lode parameter (L)

Variance source	DF	Sum of squares (SS)	Mean squares (MS)	F-Value	p-Value	% contribution of p
Model	6	0.003080	0.000513	60.61	0.098	99.708
l	1	0.000155	0.000155	18.30	0.146	5.018
w	1	0.002636	0.002636	311.17	**0.036**	85.335
r	1	0.000148	0.000148	17.50	0.149	4.791
*l*w*	1	0.000082	0.000082	9.68	0.198	2.654
*l*r*	1	0.000011	0.000011	1.34	0.454	0.356
*w*r*	1	0.000048	0.000048	5.69	0.253	1.554
Error	1	0.000008	0.000008			0.259
Total	7	0.003089				100

References

ARAMIS, 2009. User Manual—Software. v6.1 Rev, b ed. GOM mbH, Braunschweig, Germany.

Arsene, S., Bai, J., 1996. A new approach to measuring transverse properties of structural tubing by a ring test. J. Test. Eval. 24, 386. https://doi.org/10.1520/JTE11461J.

Arzaghi, M., Fundenberger, J.J., Toth, L.S., Arruffat, R., Faure, L., Beausir, B., Sauvage, X., 2012. Microstructure, texture and mechanical properties of aluminum processed by high-pressure tube twisting. Acta Mater. 60, 4393–4408. https://doi.org/10.1016/j.actamat.2012.04.035.

ASTM D2290, 2003. Standard Test Method for Apparent Hoop Tensile Strength of Plastic or Reinforced Plastic Pipe by Split Disk Method. ASTM International, West Conshohocken, PA, USA.

Bahloul, R., Mkaddem, A., Dal Santo, P., Potiron, A., 2006. Sheet metal bending optimisation using response surface method, numerical simulation and design of experiments. Int. J. Mech. Sci. 48, 991–1003. https://doi.org/10.1016/j.ijmecsci.2006.03.004.

Barsoum, I., Al Ali, K.F., 2015. A procedure to determine the tangential true stress-strain behavior of pipes. Int. J. Pres. Ves. Pip. 128, 59–68. https://doi.org/10.1016/j.ijpvp.2014.11.002.

Bates, D.W., Koss, D.A., Motta, A.T., Majumdar, S., 2000. Influence of specimen design on the deformation and failure of zircaloy cladding. Int. Top. Meet. Light Water React. Fuel Perform. 19, 1201–1210.

Bouvier, S., Haddadi, H., Levée, P., Teodosiu, C., 2006. Simple shear tests: experimental techniques and characterization of the plastic anisotropy of rolled sheets at large strains. J. Mater. Process. Technol. 172, 96–103. https://doi.org/10.1016/j.jmatprotec.2005.09.003.

Box, G.E.P., Behnken, D.W., 1960. Some new three level designs for the study of quantitative variables. Technometrics 2, 455–475. https://doi.org/10.1080/00401706.1960.10489912.

Burden, F., Winkler, D., 2008. Bayesian Regularization of Neural Networks. In: Livingstone, D.S. (Ed.), Artificial Neural Networks: Methods and Protocols. Humana Press.

Cohen, A.B., Majumdar, S., Ruther, W.E., Billone, M.C., Chung, H.M., Neimark, L.A., 1998. Modified Ring Stretch Tensile Testing of Zr-1Nb Cladding, Nuclear Regulatory Commission. Office of Nuclear Regulatory Research, Washington, DC (USA). https://doi.org/10.2172/305919.

Daum, R.S., Majumdar, S., Tsai, H., Bray, T.S., Koss, D.A., Motta, A.T., Billone, M.C., 2002. Mechanical property testing of irradiated zircaloy cladding under reactor transient conditions. In: Sokolov, J. Landes, Lucas, G. (Eds.), Small Specimen Test Techniques: Fourth Volume, 195-210. ASTM International, West Conshohocken, PA, USA. https://doi.org/10.1520/STP10821S.

Derringer, G., Suich, R., 1980. Simultaneous optimization of several response variables. J. Qual. Technol. 4 (12), 214–219.

Dick, C.P., Korkolis, Y.P., 2014. Mechanics and full-field deformation study of the ring hoop tension test. Int. J. Solid Struct. 51, 3042–3057. https://doi.org/10.1016/j.ijsolstr.2014.04.023.

Dunand, M., Mohr, D., 2014. Effect of Lode parameter on plastic flow localization after proportional loading at low stress triaxialities. J. Mech. Phys. Solid. 66, 133–153. https://doi.org/10.1016/j.jmps.2014.01.008.

Grigoriev, V., Jakobsson, R., Josefsson, B., Schrire, D., 2002. Advanced techniques for mechanical testing of irradiated cladding materials. In: Advanced Techniques for Mechanical Testing of Irradiated Cladding Materials.

Gruben, G., Fagerholt, E., Hopperstad, O.S., Børvik, T., 2011. Fracture characteristics of a cold-rolled dual-phase steel. Eur. J. Mech. Solid. 30, 204–218. https://doi.org/10.1016/j.euromechsol.2011.01.004.

Hambli, R., 2002. Prediction of burr height formation in blanking processes using neural network. Int. J. Mech. Sci. 44, 2089–2102. https://doi.org/10.1016/S0020-7403(02)00168-6.

He, Z., Yuan, S., Liu, G., Wu, J., Cha, W., 2010. Formability testing of AZ31B magnesium alloy tube at elevated temperature. J. Mater. Process. Technol. 210, 877–884. https://doi.org/10.1016/j.jmatprotec.2010.01.020.

Islam, R., Haghshenas, M., 2019. Statistical optimization of stress level in Mg-Li-Al alloys upon hot compression testing. J. Magnes. Alloy 7, 203–217. https://doi.org/10.1016/j.jma.2019.03.003.

Jiang, L., Jonas, J.J., Boyle, K., Martin, P., 2008. Deformation behavior of two Mg alloys during ring hoop tension testing. Mater. Sci. Eng. 492, 68–73. https://doi.org/10.1016/j.msea.2008.04.028.

Kalmegh, A.P., Khodke, P.M., 2018. Design of experimentation for composite desirability of low plasticity burnishing process for AISI 4340. Int. J. Pure Appl. Math. 120, 10221–10235.

Kim, J., Kim, Youngjun, Kim, Yongsoo, 2012. A study on the zircaloy ring tensile test. In: Transactions of the Korean Nuclear Society Spring Meeting, pp. 17–18.

Kim, S.K., Bang, J.G., Kim, D.H., Lim, I.S., Yang, Y.S., Song, K.W., Kim, D.S., 2009. Hoop strength and ductility evaluation of irradiated fuel cladding. Nucl. Eng. Des. 239, 254–260. https://doi.org/10.1016/j.nucengdes.2008.10.024.

Lee, M.H., Kim, J.H., Park, S.Y., Choi, B.K., Jeong, Y.H., 2009. The circumferential tensile properties of zirconium alloy fuel claddings under a simulated high burn-up environment. Met. Mater. Int. 15, 539–546. https://doi.org/10.1007/s12540-009-0539-0.

Lin, Y.L., He, Z. Bin, Yuan, S.J., Wu, J., 2011. Formability determination of AZ31B tube for IHPF process at elevated temperature. Trans. Nonferrous Metals Soc. China 21, 851–856. https://doi.org/10.1016/S1003-6326(11)60792-9.

Link, T.M., Koss, D.A., Motta, A.T., 1998. Failure of zircaloy cladding under transverse plane-strain deformation. Nucl. Eng. Des. 186, 379–394. https://doi.org/10.1016/S0029-5493(98)00284-2.

Martín-Rengel, M.A., Gómez Sánchez, F.J., Ruiz-Hervías, J., Caballero, L., Valiente, A., 2012. Revisiting the method to obtain the mechanical properties of hydrided fuel cladding in the hoop direction. J. Nucl. Mater. 429, 276–283. https://doi.org/10.1016/j.jnucmat.2012.06.003.

MATLAB, 2010. Neural Network Toolbox™ 7, Release. The MathWorks, Natick, Massachusetts, Inc, USA.

Mehan, R.L., Jackson, M.R., Rairden, J.R., Carter, W.T., 1987. The use of a ring tensile test to evaluate plasma-deposited metals. J. Mater. Sci. 22, 4476–4483. https://doi.org/10.1007/BF01132050.

Nagase, F., Sugiyama, T., Fuketa, T., 2009. Optimized ring tensile test method and hydrogen effect on mechanical properties of zircaloy cladding in hoop direction. J. Nucl. Sci. Technol. 46, 545–552. https://doi.org/10.1080/18811248.2007.9711560.

Pereira, A.F.G., Prates, P.A., Sakharova, N.A., Oliveira, M.C., Fernandes, J.V., 2015. On the identification of kinematic hardening with reverse shear test. Eng. Comput. 31, 681–690. https://doi.org/10.1007/s00366-014-0369-7.

Pierron, O.N., Koss, D.A., Motta, A.T., 2003. Tensile specimen geometry and the constitutive behavior of zircaloy-4. J. Nucl. Mater. 312, 257–261. https://doi.org/10.1016/S0022-3115(02)01554-4.

Prasad, B.S., Babu, M.P., 2017. Correlation between vibration amplitude and tool wear in turning: numerical and experimental analysis. Eng. Sci. Technol. Int. J. 20, 197–211. https://doi.org/10.1016/j.jestch.2016.06.011.

Prates, P.A., Oliveira, M.C., Fernandes, J.V., 2014. A new strategy for the simultaneous identification of constitutive laws parameters of metal sheets using a single test. Comput. Mater. Sci. 85, 102–120. https://doi.org/10.1016/j.commatsci.2013.12.043.

Price, E.G., 1972. Hydride orientation and tensile properties of Zr-2.5wt%Nb pressure tubing hydrided while internally pressurized. Can. Metall. Q. 11, 129–138. https://doi.org/10.1179/cmq.1972.11.1.129.

Saikaly, W.E., Bailey, W.D., Collins, L.E., 1996. Comparison of ring expansion vs flat tensile testing for determining linepipe yield strength. Proc. Int. Pipeline Conf. IPC 1, 209–213. https://doi.org/10.1115/ipc1996-1825.

Samal, M.K., Balakrishnan, K.S., Parashar, J., Tiwari, G.P., Anantharaman, S., 2013. Estimation of transverse tensile behavior of zircaloy pressure tubes using ring-tensile test and finite element analysis. Proc. Inst. Mech. Eng. Part C. J. Mech. Eng. Sci. 227, 1177–1186. https://doi.org/10.1177/0954406212460474.

Sarikaya, M., Güllü, A., 2014. Taguchi design and response surface methodology based analysis of machining parameters in CNC turning under MQL. J. Clean. Prod. 65, 604–616. https://doi.org/10.1016/j.jclepro.2013.08.040.

Seok, C.S., Bae, B.K., Koo, J.M., Murty, K.L., 2006. The properties of the ring and burst creep of ZIRLO cladding. Eng. Fail. Anal. 13, 389–397. https://doi.org/10.1016/j.engfailanal.2005.02.009.

Souto, N., Andrade-Campos, A., Thuillier, S., 2014. Mechanical design of a heterogeneous test for material parameters identification. Int. J. Material Form. 10, 353–367. https://doi.org/10.1007/s12289-016-1284-9.

Wang, H., Bouchard, R., Eagleson, R., Martin, P., Tyson, W., 2002. Ring hoop tension test (RHTT): a test for transverse tensile properties of tubular materials. J. Test. Eval. 30, 382. https://doi.org/10.1520/JTE12328J.

Yoshitake, T., Abe, Y., Akasaka, N., Ohtsuka, S., Ukai, S., Kimura, A., 2004. Ring-tensile properties of irradiated oxide dispersion strengthened ferritic/martensitic steel claddings. J. Nucl. Mater. 329, 342–346. https://doi.org/10.1016/j.jnucmat.2004.04.084.

Zaddem, M., 2014. Application de la méthode des surfaces de réponse pour l'optimisation du blanchiment du son de blé par du peroxyde d'hydrogène et son incorporation dans une farine de pain. Laval University, Dissertation.

Zribi, T., Khalfallah, A., Belhadjsalah, H., 2013. Experimental characterization and inverse constitutive parameters identification of tubular materials for tube hydroforming process. Mater. Des. 49, 866–877. https://doi.org/10.1016/j.matdes.2013.02.077.